Spectrum of coherent synchrotron radiation in the far-infrared region

K. Ishi, Y. Shibata, T. Takahashi, H. Mishiro, T. Ohsaka, and M. Ikezawa
Research Institute for Scientific Measurements, Tohoku University, Katahira Aoba-ku Sendai 980, Japan

Y. Kondo
Department of Applied Physics, Faculty of Engineering, Tohoku University, Aramaki Aoba-ku Sendai 980, Japan

T. Nakazato, S. Urasawa, N. Niimura, R. Kato, Y. Shibasaki, and M. Oyamada
Laboratory of Nuclear Science, Tohoku University, Mikamine Taihaku-ku Sendai 982, Japan
(Received 13 November 1990)

A spectrum of coherent synchrotron radiation emitted from a bunch train of relativistic electrons accelerated by the Tohoku 300-MeV linear accelerator (linac) has been observed in the wavelength range from 0.16 to 3.5 mm. The energy of the electrons and the longitudinal bunch length are 150 MeV and about 2 mm. The observed spectrum has a broad peak at $\lambda \simeq 1.5$ mm, and the intensity decreases sharply towards shorter wavelengths. The peak intensity is enhanced by a factor of 5×10^6 in comparison with ordinary incoherent synchrotron radiation; the enhancement factor is comparable with the average number of electrons in the bunch. The electron distribution in the bunch is derived from the observed spectrum, and the bunch length (full width at half maximum) is obtained to be 0.25 mm. This bunch length is shorter than that estimated from the characteristics of the linac. The relation between the spectrum and the distribution of electrons in the bunch is discussed.

I. INTRODUCTION

Electron bunches in storage rings radiate light pulses of ordinary incoherent synchrotron radiation (SR) over a wide frequency range from the radio frequency to the ultraviolet or x-rays. SR is an excellent light source for uv, x-ray, and far-infrared spectroscopy because it has high brightness, high stability, clean environment, pulsed time structure, and high polarization over the wide and continuous spectral range.[1-6] Incoherent SR from the storage ring is now regarded as a standard light source.

In the region where the wavelength is as long as the mean distance between electrons in a bunch, SR will be partially coherent.[7,8] In such a case, the intensity of SR depends not only on the number of accelerated electrons, but on the bunch length and the electron distribution in the bunch.

At the early stages of development of the synchrotron, several authors[7,8] studied the increase of energy loss due to a coherence effect of SR. Schiff[7] gave the expression of the loss, or the emission rate of SR, for the case in which the electrons are spread in a Gaussian distribution about the equilibrium phase. Nodvick and Saxon[8] have given the expression of the spectral intensity of coherent SR. More recently, a possibility of submillimeter coherent radiation in electron storage rings was pointed out theoretically by Michel[9] in 1982 and was discussed by Wingham[10] in 1987.

According to the theory,[7-10] the intensity of SR has been expected to be greatly enhanced due to the coherence effect, when the wavelength is longer than the longitudinal bunch length. The enhancement factor is nearly equal to the number of electrons in the bunch, in comparison with that of ordinary incoherent SR.

A positive indication of the coherence effect of SR was reported by Yarwood *et al.*[4] in 1984 who used the Synchrotron Radiation Source (SRS) at Daresbury. However, coherent SR from storage rings has not been conclusively confirmed. Schweizer *et al.*[5] were unable to detect any enhancement in the wavelength range from 1 to 667 μm at the storage ring BESSY with a bunch length of about 3 cm. Williams *et al.*[11] could observe no enhancement in the wavelength range from 30 to 400 μm, using the BNL National Synchrotron Light Source ring with a bunch length of 30 cm. Nanba *et al.*[12] also obtained a negative result in the millimeter region with a bunch length of 6 cm at the Ultraviolet Synchrotron Orbital Radiation (UVSOR) facility of the Institute for Molecular Science. In these experiments the observed wavelengths were much shorter than the bunch lengths.

In 1989 using the Tohoku 300-MeV linear accelerator (linac), the coherence effect of SR was observed for the first time by our group[13-15] in the far-infrared region. The electron energy from the linac was 180 MeV and the bunch length was estimated to be about 2 mm. The intensity of coherent SR was about 1.0×10^6 times as strong as that expected for incoherent radiation at the wavelengths around 1 mm. The value of the enhancement factor was the same order of magnitude as N_e, the number of electrons in the bunch. The intensity of coherent SR was proportional to N_e^2 and the radiation was mainly polarized in the orbital plane. Coherent SR from the electron bunches of the linac can be used as a useful light source in the submillimeter and millimeter wavelength region.

The measurement of the spectrum of coherent SR over wide spectral ranges is important to investigate not only the electron distribution in the bunch but also the radia-

tion mechanism of coherent SR. In the previous experiments, we were unable to observe the full spectrum in the submillimeter region, because optical filters were incomplete to eliminate stray light of intense coherent SR. The purpose of this work is to obtain a precise spectrum of coherent SR in a wide wavelength region and to study the relation between the spectrum and the electron distribution in the bunch. For this purpose a far-infrared spectrometer has been constructed, which was equipped with short-wavelength-pass filters to cut off the stray light of the long wavelengths.

II. THEORY OF COHERENT SR FROM BUNCH TRAIN

Several authors have studied coherent SR from bunched electrons.[7,8] Recently, however, the interference effect of SR between successive bunches was experimentally proved to be important.[16] In this section, we present a simple theory for the analysis of the present experiment. The interference effect was also treated by Wingham.[10]

Here, we consider a train of light pulses of SR emitted from a train of bunched electrons. In the experiment, as shown in Fig. 1 and Table I, the observation point is far from the emitting point of SR. Let x be a curvilinear coordinate along the circular orbit, and $p(\lambda)=|E_0(\lambda)|^2$ be the intensity of SR at wavelength λ emitted by a single electron.[17] Then, the electric field at the observation point from the successive bunches can be expressed as

$$E_T(\lambda)=E_0(\lambda)\sum_{j=1}^{N_B}\left[\sum_{n=1}^{N_e}\exp\left[-i2\pi\frac{x_n^j-c(j-1)\tau}{\lambda}\right]\right], \tag{1}$$

where N_e, N_B, and τ stand for the number of electrons in a bunch, total number of bunches, and the time interval between the successive bunches, respectively. The quantity x_n^j gives the position of the nth electron in the jth bunch relative to the bunch center. The time interval τ was assumed to be constant, as the accelerating rf of the linac was stable enough in the present experiment. The intensity of SR from one bunch, which includes N_e electrons, is given by[8]

$$\begin{aligned}P_{\rm coh}(\lambda)&=|E_T(\lambda)_{N_B=1}|^2\\&=p(\lambda)N_e[1+(N_e-1)f(\lambda)]\\&\sim p(\lambda)N_e^2 f(\lambda)\ ,\end{aligned} \tag{2}$$

$$f(\lambda)=\left|\int\exp\left[i2\pi\frac{x}{\lambda}\right]S(x)dx\right|^2\ , \tag{3}$$

where $f(\lambda)$ is a bunch form factor defined by the Fourier transform of $S(x)$, the density distribution function of an electron in a bunch. The value of the bunch form factor varies from zero at wavelengths $\lambda\ll x$ (incoherent limit) to unity at $\lambda\gg x$ (coherent limit).

The distribution function is calculated by the inverse transformation of the bunch form factor. By the definition, the bunch form factor Eq. (3) has the symmetry $f(-\lambda)=f(\lambda)$. Therefore the inverse transformation of $f(\lambda)$ gives only the even component of the distribution function,

$$S(x)=\int f(\lambda)^{1/2}\cos\left[2\pi\frac{x}{\lambda}\right]d\lambda\ . \tag{4}$$

Thus the electron distribution obtained from the observed spectrum is a symmetric function of the coordinate x.

The total intensity of coherent SR from N_B bunches is given by

$$P_{\rm coh}(\lambda)=p(\lambda)\langle N_e^2 f(\lambda)\rangle G(\lambda)\ , \tag{5}$$

$$\begin{aligned}G(\lambda)&=\left|\sum_{j=1}^{N_B}\exp\left[i2\pi(j-1)\frac{L_B}{\lambda}\right]\right|^2\\&=\left[\frac{\sin(\pi L_B N_B/\lambda)}{\sin(\pi L_B/\lambda)}\right]^2\ .\end{aligned} \tag{6}$$

The angular brackets show a mean value averaged over the bunches. The interference effect between the successive bunches is given by the factor $G(\lambda)$, and the quantity L_B stands for the distance between the successive bunches. Equation (5) corresponds to the coherent component given by Eq. (4.16) in Wingham's paper.[10]

The theoretical spectral intensity given by Eq. (5) includes a rapidly oscillating factor with the wavelength. When $N_B\gg1$, the spectrum consists of a series of lines. Frequencies of the lines correspond to the higher harmonics of the fundamental frequency defined by $\nu_B=c/L_B$, i.e., the rf of the linac, 2856 MHz in the present experiment. The interference effect can be measured only with an apparatus whose resolution is higher than ν_B.

When resolution of a spectrometer is lower than ν_B, an observed spectrum results in a mean value of intensity averaged over a wavelength interval corresponding to the resolution of the apparatus. When $N_B\gg1$, the function $G(\lambda)$ varies so rapidly that the other functions in Eq. (5) are considered to be constant for the narrow wavelength interval. Let k be an arbitrary integer; then the mean intensity at the wavelength $\lambda=L_B/(k+\frac{1}{2})$ is given by

$$\begin{aligned}P_{\rm coh}(\lambda)&=p(\lambda)\langle N_e^2 f(\lambda)\rangle L_B\int_{L_B/k}^{L_B/(k+1)}G(\lambda')d\lambda'\\&=p(\lambda)\langle N_e^2 f(\lambda)\rangle N_B\ .\end{aligned} \tag{7}$$

Thus the intensity of the low-resolution spectrum of coherent SR from a bunch train is equal to the spectral intensity from a single bunch multiplied by the number of bunches.

III. EXPERIMENT

A. Generation of coherent SR

The experimental assembly is shown in Fig. 1. The electron beam was accelerated up to the energy of 150 MeV by the Tohoku 300-MeV linac. The accelerating rf was 2856 MHz. A magnetic field of 0.206 T was applied

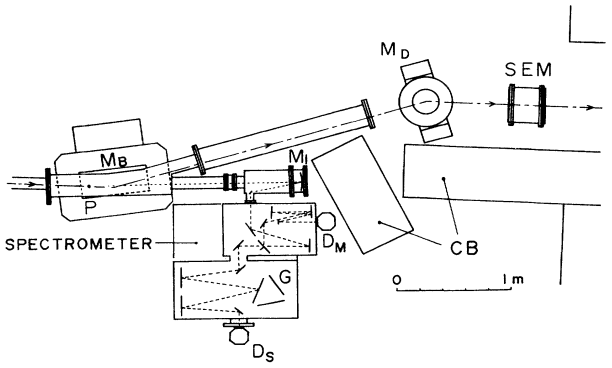

FIG. 1. The experimental assembly. P, light emitting point of SR; M_B, bending magnet; M_D, dumping magnet; SEM, secondary emission monitor; M_1, collecting mirror; G, gratings; D_S, detector for signal; D_M, detector for monitor; and CB, concrete blocks for radiation shield. Trajectory of bunched electron beam is shown by a chain line.

to the electron beam to produce SR. Source characteristics of SR are given in Table I. A bending radius of the electron orbit and the characteristic wavelength of SR were 2.44 m and 404 nm, respectively. A duration of the bunch train was 2 μs and its repetition was 300 pulse/sec. An average beam current was measured by a secondary emission monitor downstream from the bending magnet. From the characteristics of the linac,[13,18] the longitudinal bunch length was estimated to be about 2 mm at the light emitting point, where the transverse bunch size was about 2×2 mm^2 and the beam energy spread was 0.2%. The number of electrons in the bunch was 3.6×10^6 at an average beam current of 1 μA.

Coherent SR can be suppressed in part by the use of metallic shields.[8] In order to avoid the shielding effect in the wavelength range observed here, the cross-sectional dimensions of the vacuum duct were designed to be as large as 200×200 mm^2 at the emission point.

Emitted SR was collected by a spherical mirror with an acceptance angle of 70 mrad, and was led to the far-infrared spectrometer described in the next section.

TABLE I. Source characteristics of synchrotron radiation.

Electron beam	
Electron energy	150 MeV
Energy width	0.2%
Repetition	300 Hz
Radio frequency	2856 MHz
Bending radius of electron orbit	2.44 m
Beam size (horizontal$\times$vertical)	
at emission point P	2×2 mm^2
at 2.64 m downstream point from P	9.5×6.5 mm^2
Acceptance of synchrotron radiation	
Distance between emission point and collecting mirror	1.88 m
Acceptance angle of collecting mirror	70 mrad

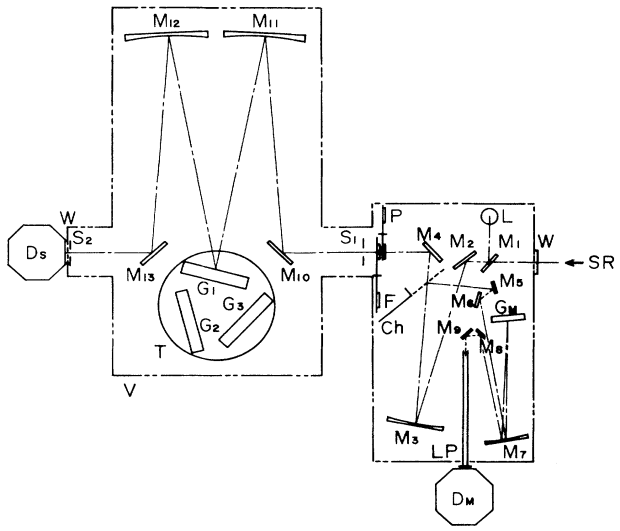

FIG. 2. The optical layout of spectrometer. M_1, M_2, M_5, M_6, M_8, M_9 M_{10}, and M_{13}, plane mirror; M_3, spherical mirror; M_4, scatter plate; M_7, collimator mirror for monitor; M_{11}, collimator mirror; M_{12}, telescope mirror; L, high-pressure mercury arc lamp; Ch, chopper mirror; P, polarizer and shutter; F, filter set; S_1 and S_2, entrance and exit slits; G_1, G_2, and G_3, gratings; G_M, grating for monitor; LP, light pipe; T, turntable; D_S, detector for signal; D_M, detector for monitor; V, vacuum tank; W, quartz window; and SR, synchrotron radiation.

B. Spectrometer

The grating-type far-infrared spectrometer was constructed, which had metal mesh filters to cut off the stray light accompanied with intense coherent SR in the long-wavelength region. It had a system to monitor the fluctuation of the intensity due to the instability of electron beam. All optical components were in a vacuum tank to eliminate the absorption loss by water vapor.

The optical layout of the spectrometer is illustrated in Fig. 2. Coherent SR is imaged onto an entrance slit of the monochromator. The dispersive system is an $f/4.8$ Czerny-Turner type. Spherical mirrors of 750 mm focal length are used as a collimator mirror and a telescope mirror. Five echelette gratings of 5, 2.5, 1.25, 0.625, and 0.3125 grooves/mm are used to cover the wavelength range from 0.1 to 4.0 mm. Each grating has a 154×128 mm^2 effective ruled area. Three gratings can be mounted on a turnable. Scanning is made by a high-precision pulse motor connected directly with the turntable. The signal is detected by a liquid-helium-cooled silicon bolometer with three long-wavelength-pass filters and is transmitted to an amplifier. The radiation reflected by a 10-Hz chopper mirror is converged onto a liquid-helium-cooled silicon bolometer of the monitoring system.

The combinations of filters and grating adopted for each spectral range are listed in Table II. Transmission spectra of the metal meshes, which were found to be effective long-wavelength-cut filters, are shown in Fig. 3. The control of the spectrometer and data acquisition were made by a computer (NEC Co. PC-9801).

TABLE II. Combinations of optical elements for each spectral range.

Spectral range (μm)	Grating (lines/mm)	Filter: LWPF[a]	Filter: SWPF[b] (mesh number)	Filter: LWPF[a] of detector cutoff wavelength (μm)
~100–125	5	(NaCl+KCl+NaF+Cu_2O+polyethylene) +crystalline quartz	40	100
~125–167	5	(KBr+BaF_2+Cu_2O+polyethylene) +crystalline quartz	40	100
~167–222	5	($CaCO_3$+KBr+BaF_2+Cu_2O+polyethylene) +crystalline quartz	40	100
~222–333	2.5	($CaCO_3$+KBr+BaF_2+Cu_2O+polyethylene) +(TlCl+TlI+NaF+polyethylene) +crystalline quartz	200	100
~333–500	1.25	300 μm (cutoff wavelength)	80	286
~500–1000	1.25	500 μm (cutoff wavelength)	50	286
~1000–2000	0.625	1000 μm (cutoff wavelength)	24	286
~2000–4000	0.3125	1000 μm (cutoff wavelength)	24	286

[a]Long-wavelength-pass filter.
[b]Short-wavelength-pass filter of metal mesh.

C. Intensity calibration

The absolute sensitivity of the measuring system was calibrated by a blackbody radiator at 1500±1 K, which was located at the emission point of SR. The structure of the blackbody radiator is shown in Fig. 4. The radiator was made up from a graphite cavity, and the effective aperture is 12 mm. In order to obtain a high signal-to-noise ratio, the measurements for calibration were repeated 40 times at maximum, because the intensity of the blackbody radiation at 1500 K was extremely weak at wavelengths longer than 1 mm. The accuracy of the absolute intensity of coherent SR after the correction was estimated to be within a factor of 1.5.

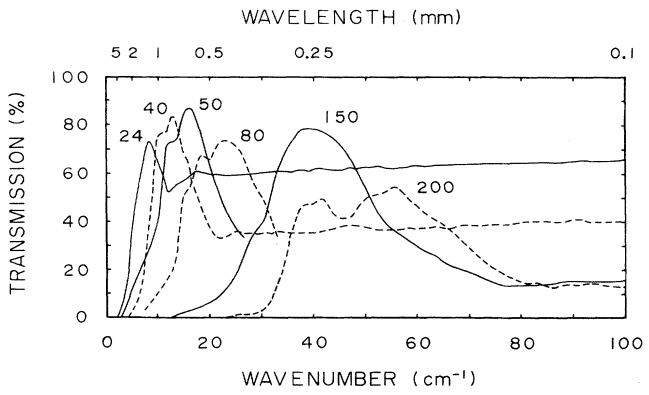

FIG. 3. The transmission spectra of metal mesh filters. The mesh number is given in the figure.

IV. EXPERIMENTAL RESULTS

A. Spectrum

The spectrum of coherent SR was observed in the wavelength range from 0.16 to 3.5 mm. The observed spectrum is shown in Fig. 5. The spectrum shows a broad peak at $\lambda \simeq 1.5$ mm, and the peak intensity is enhanced by a factor of 5×10^6 in comparison with ordinary incoherent SR. The enhancement factor is comparable with the number of electrons in the bunch, 3.6×10^6. In the wavelength range $\lambda < 0.5$ mm, the spectral intensity decreases rapidly as the wavelength decreases. As is shown in Table II, the longest cutoff wavelength of the long-wavelength-pass filter was 1 mm; hence the order separation might be insufficient in the range $\lambda > 2$ mm. However, the spectrum at wavelengths $\lambda > 2$ mm seems to be hardly affected by the unwanted light, since a spectrum recently observed by a polarizing interferometer showed a similar spectrum in the range $\lambda > 2$ mm.[16] In the narrow wavelength ranges $1.38 < \lambda < 1.56$ mm and $0.20 < \lambda < 0.22$ mm in Fig. 5, the spectrum was not correctly observed for the following reasons. In the range $1.38 < \lambda < 1.56$ mm, the long-wavelength-pass filter used (see Table II) did not sufficiently cut off unwanted higher-order light of shorter wavelengths. In the range $0.20 < \lambda < 0.22$ mm, where the efficiency of a grating used was low, the intensity of coherent SR was too weak to be observed. Intensities in these ranges were linearly interpolated (see Fig. 6) to derive the bunch form factor from the observation as given in a later section.

The theoretical spectrum given by Eq. (5) has an oscillating structure with a period of 2856 MHz (0.095 cm^{-1}) in the present experiment. The resolution of the spectrometer was about 0.1 cm^{-1} at $\lambda \sim 1$ mm. However, the

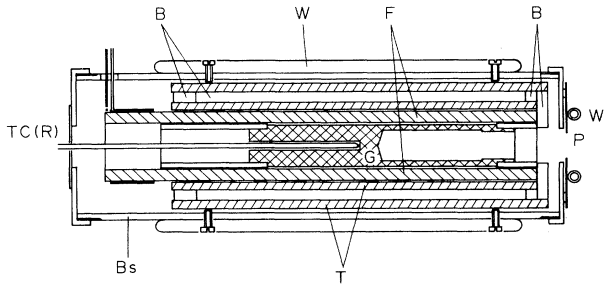

FIG. 4. The blackbody radiator. *F*, siliconit heater; *G*, graphite cavity; *T*, alumina tubes; *B*, heat insulating material; Bs, brass tube; TC, thermocouple; *P*, field stop; and *W*, water cooling pipe.

oscillation was not observed, probably for the following reason. In the measurement of the spectrum, the scanning interval was about 0.035 cm^{-1} on the average at $\lambda \sim 1.5$ mm and was not constant in the frequency scale. Moreover, the sampling points were taken irrespectively of the period of the oscillation and might have overlapped fortuitously with the local maxima of the oscillation. This sampling interval was inadequate to find out the oscillation from the observed spectrum including experimental errors. We consider that the averaged spectrum given by Eq. (7) has been observed in the present experiment.

B. Bunch form factor

The bunch form factor was derived from the observed spectrum by applying Eq. (7). The result is shown in Fig. 6. The overall structure of the bunch form factor resembles the observed spectrum, since $p(\lambda)$ is a slowly varying function proportional to $\lambda^{-1/3}$ in the far-infrared region.[3] In Fig. 6, the bunch form factor predicted by Michel[9] is also shown by a straight line broken at $\lambda=2$ mm. This has a wavelength dependence of λ^3 in the shorter wavelength region. The wavelength dependence of the observed bunch form factor is almost λ^6 in the range from 0.16 to 0.5 mm (shown as a dashed line in Fig. 6). The experimental result disagrees with Michel's theory.

The bunch form factor should have the upper limit of unity. On the other hand, the observed bunch form factor is larger than unity at around the peak wavelengths. This discrepancy may be caused by the following uncertainty, in addition to the experimental errors of the calibrated intensity. In the conversion process by Eq. (7), it was assumed implicitly that $\langle N_e^2 f(\lambda)\rangle = \langle N_e\rangle^2 \langle f(\lambda)\rangle$. The electron beam from the linac shows temporal variation over the duration of the bunch train, so that $\langle N_e^2\rangle$ is always larger than $\langle N_e\rangle^2$; it makes the experimentally obtained bunch form factor large.

C. Electron distribution in a bunch

The electron distribution derived from the observed spectrum by Eq. (4) is shown in Fig. 7. The bunch shape resembles a Gaussian function with a sharp peak. The longitudinal bunch length (full width at half maximum) is about 0.25 mm, which is shorter than the bunch length of 2 mm estimated from the characteristics of the linac.[13,18]

Figure 7 shows that electrons are confined in a short arc along the circular orbit, $|x| < 0.4$ mm. Hence, according to the asymptotic property of Eq. (3), the bunch form factor in the range $\lambda > 1.6$ mm should increase monotonically to unity, as the wavelength increases. On the contrary, the observed bunch form factor decreases towards longer wavelengths. Though the suppression of SR by the shielding effect[8] at around $\lambda=4$ mm is estimat-

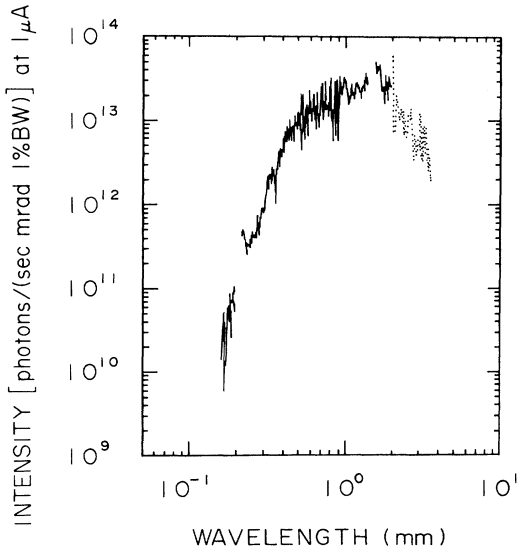

FIG. 5. The observed spectrum of coherent SR. The intensity is calibrated by a blackbody radiation of 1500 K.

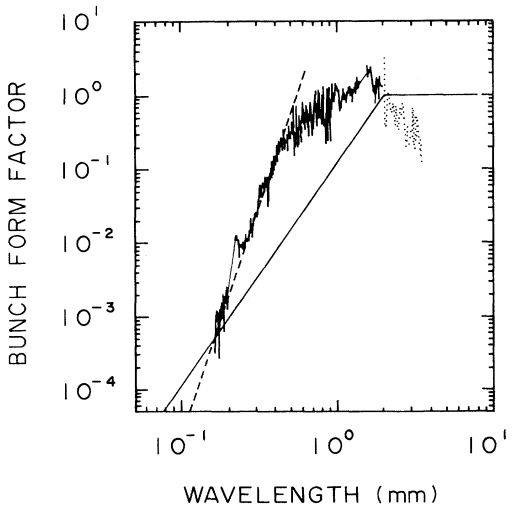

FIG. 6. The bunch form factor derived from the observed spectrum. The straight line bent at $\lambda=2$ mm shows the relation by Michel (Ref. 9).

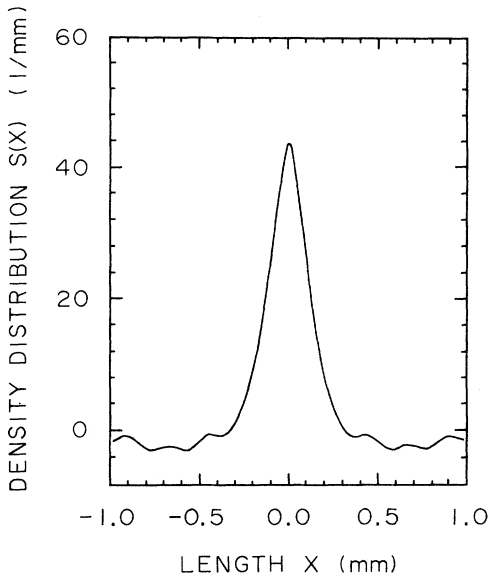

FIG. 7. The electron distribution function $S(x)$ in the bunch obtained from the observed spectrum.

ed to be small, the shielding effect may be a possible cause of the decrease. The decrease may also be explainable by a broad, e.g., $|x| \simeq 1.5$ mm, distribution of electrons, in addition to a sharp concentration as discussed below.

V. DISCUSSION

According to the accelerating mechanism of electrons by the linac, it is possible that the electron distribution has sharp local concentrations in the bunch. Moreover, the distribution function obtained by Eq. (4) is only the even function. To examine the relation between the electron distribution and the spectrum shape, a model calculation has been carried out. The distribution function $S(x)$ is assumed to be given by two Gaussian components, to include the effects of local concentration and the asymmetric distribution. We write

$$S(x)=\frac{1}{2\pi^{1/2}}\left[\frac{\alpha}{D_1}\exp\left[-\frac{(x-L)^2}{2D_1^2}\right]+\frac{1-\alpha}{D_2}\exp\left[-\frac{x^2}{2D_2^2}\right]\right], \tag{8}$$

where D_1 and α are the dispersion and the fractional weight of the distribution given by the first term, and D_2 and $1-\alpha$ are those by the second term, and L is the distance between the two peaks. The function $S(x)$ gives a symmetric distribution if (1) $L=0$, or (2) $D_1=D_2$ and $\alpha=0.5$. Otherwise, $S(x)$ is asymmetric.

Then, the bunch form factor is calculated by Eq. (3). We write

$$f(\lambda)=\alpha^2\exp\left[-\left[\frac{2\pi D_1}{\lambda}\right]^2\right]+(1-\alpha)^2\exp\left[-\left[\frac{2\pi D_2}{\lambda}\right]^2\right]+2\alpha(1-\alpha)\cos\left[\frac{2\pi L}{\lambda}\right]\exp\left[-2\pi^2\frac{D_1^2+D_2^2}{\lambda^2}\right]. \tag{9}$$

The third term in Eq. (9) shows an oscillation with the period of $\Delta\nu=c/L$. The amplitude decreases as the wavelength decreases. The first minimum occurs at $\lambda=2L$.

Model calculations have been carried out for various parameters. Figures 8 and 9 show examples of the calculation; Fig. 8 shows the electron distribution functions and Fig. 9 the calculated bunch form factors. The solid line in Fig. 8 shows the symmetric distribution given by two equicenter Gaussian functions. The dotted line gives the asymmetric distribution; a sharp peak is superposed on a broad peak at a position near the limb. A Gaussian function with the dispersion of 0.1 mm is also given by the dashed line.

Results of the calculation are summarized as follows.

(1) A local concentration of electrons in longitudinal size of about 0.2 mm is necessary to explain the sharp decrease of the observed intensity in the region $\lambda<0.5$ mm towards shorter wavelengths, irrespective to the peak position in the bunch.

(2) A fairly large portion of electrons in the bunch should be confined in the local concentration. Otherwise, the spectral intensity observed in Fig. 6 in the range $0.5<\lambda<2$ mm is not explainable.

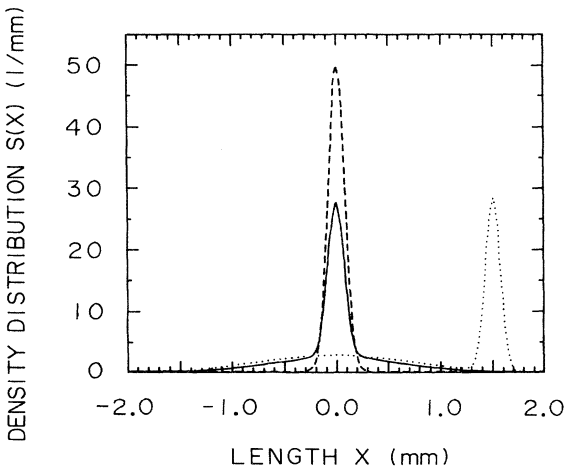

FIG. 8. The electron distribution function $S(x)$. The parameters in Eq. (8) are as follows; (1) symmetric distribution, $D_1=0.1$ mm, $D_2=1.0$ mm, $\alpha=0.5$, $L=0$ for the solid line, and (2) asymmetric distribution, $D_1=0.1$ mm, $D_2=1.0$ mm, $\alpha=0.4$, $L=1.5$ mm for the dotted line. The single Gaussian distribution function; $D_1=0.1$ mm, $\alpha=1.0$ ($L=0$), is also given by the dashed line.

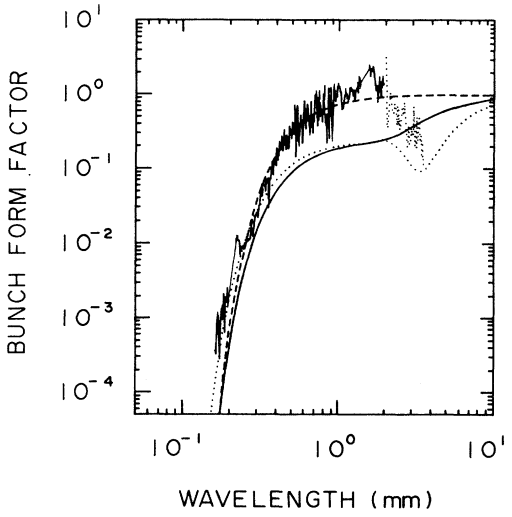

FIG. 9. The calculated bunch form factor. The observed bunch form factor is also given. The form factor was calculated by Eq. (3) in the text for distribution function given in Fig. 8. The solid and dashed lines correspond to the symmetric distribution given by the solid and dashed lines in Fig. 8, respectively. The dotted line corresponds to the asymmetric distribution given by the dotted line in Fig. 8.

(3) The decrease of the observed bunch form factor at $\lambda > 2$ mm towards longer wavelengths could be qualitatively reproduced by a two-peak distribution with $L > 1.5$ mm.

In comparison with the calculation, we may conclude that the electron distribution has at least one local concentration of electrons by longitudinal size of about 0.2 mm in the bunch. The comparison also suggests a possibility that the electron distribution has a complex structure like the one shown by a dotted line in Fig. 8.

To examine a possibility of sharp structure of the electron distribution in the bunch, the motion of electrons accelerated in the linac used has been simulated. The electron bunches are produced at the injector of the linac, which consists of an electron gun, prebuncher, buncher, and the first accelerating structure. The prebuncher is a single-cell reentrant cavity and the buncher and the first accelerating structure are traveling wave type. The accelerating parameters at the injector are shown in Table III.

In order to estimate the bunch shape, we simulated the bunching process by tracking the longitudinal motion of the electrons in the injector. The calculation was carried out according to the formulas[19]

$$\frac{d\gamma}{dz} = \frac{eE}{m_0 c^2} \sin\phi \ , \tag{10}$$

$$\frac{d\phi}{dz} = \frac{2\pi}{\lambda_0} \left[\frac{1}{\beta_w} - \frac{1}{\beta_e} \right] , \tag{11}$$

where γ $[=1/(1-\beta_e^2)^{1/2}]$ is the ratio of the total energy of the electron to rest mass energy, ϕ the phase relative to an accelerating wave with phase velocity $c\beta_w$, E the electric field gradient, λ_0 the free-space wavelength of the accelerating rf, and z is an independent variable along the beam axis.

TABLE III. Accelerating parameters at the injector of the linac. $\lambda_0 = c/2856$ MHz $= 105.0$ mm.

Electron gun	
Cathode voltage	-80 kV
Peak current	100 mA
Prebuncher	
Modulation voltage	10 kV
Drift space	$2.0\lambda_0$
Buncher	
Phase velocity	$0.7c$
Length	$2.0\lambda_0$
Electric field	2.6 MV/m
Drift space	$1.5\lambda_0$
First accelerating structure	
Phase velocity	$1.0c$
Length	$10.3\lambda_0$
Electric field	10.0 MV/m

As the energy of the electron is about 10 MeV ($\beta_e = 0.9987$) at the end of the first accelerating structure and $\beta_w = 1.0$ for the regular section of the linac, the right side of Eq. (11) can be regarded as zero downstream of the injector. Therefore the relative position among the electrons does not change so much after the injector, i.e., the bunch shape is determined in the injector.

The bunch shape depends strongly on the relative phase of the rf supplied to the prebuncher, buncher, and the first accelerating structure. One of the simulated results is shown in Fig. 10. The main body of the bunch is 1.3 mm in length and it has three spikes in it. The width of each spike is about 0.1 mm. This result is not exact but similar to our experimental bunch shape.

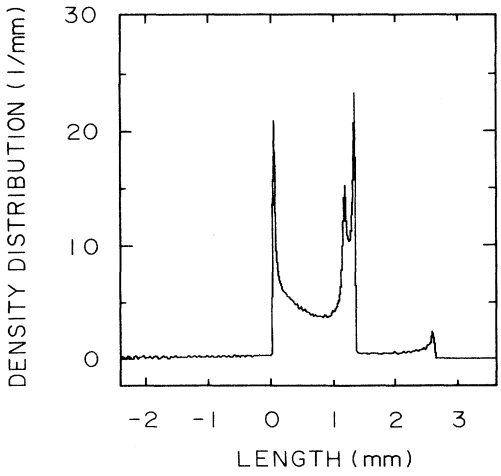

FIG. 10. An electron distribution in a bunch calculated by the simulation of motion of electrons accelerated in the injector of the linac.

The effects of the beam loading and the space charge are not taken into account in the above simulation. In order to consider these effects, a rough calculation by the one-dimensional disk model[20] was carried out. The result was almost the same as Fig. 10 because the beam intensity was small.

We consider the simulation gives qualitative but positive support to the above conclusion of the local concentration.

ACKNOWLEDGMENTS

We thank T. Tsutaya and the staff at the Laboratory of Nuclear Science for their technical support and assistance. We also express our thanks to Dr. M. Takahashi for his technical guidance on the blackbody radiation source and Professor I. Sato in National Laboratory for High Energy Physics (KEK) for offering the program code of the one-dimensional disk model.

[1]P. Lagarde, Infrared Phys. **18**, 395 (1978).
[2]J. R. Stevenson, H. Ellis, and R. Bartlett, Appl. Opt. **12**, 2884 (1973).
[3]W. D. Duncan and G. P. Williams, Appl. Opt. **22**, 2914 (1983).
[4]J. Yarwood, T. Shuttleworth, J. B. Hasted, and T. Nanba, Nature (London) **312**, 742 (1984).
[5]E. Schweizer, J. Nagel, W. Braun, E. Lippert, and A. M. Bradshaw, Nucl. Instrum. Methods A **239**, 630 (1985).
[6]T. Nanba, Y. Urashima, M. Ikezawa, M. Watanabe, E. Nakamura, K. Fukui, and H. Inokuchi, Int. J. Infrared Millimeter Waves **7**, 1769 (1986).
[7]L. I. Schiff, Rev. Sci. Instrum. **17**, 6 (1946).
[8]J. S. Nodvick and D. S. Saxon, Phys. Rev. **96**, 180 (1954).
[9]F. C. Michel, Phys. Rev. Lett. **48**, 580 (1982).
[10]D. J. Wingham, Phys. Rev. D **35**, 2584 (1987).
[11]G. P. Williams, C. J. Hirschmugl, E. M. Kneedler, P. Z. Takacs, M. Shleifer, Y. J. Chabal, and F. M. Hoffmann, Phys. Rev. Lett. **62**, 261 (1989).
[12]T. Nanba, M. Ikezawa, M. Watanabe, K. Fukui, and H. Inokuchi (unpublished).
[13]T. Nakazato, M. Oyamada, N. Niimura, S. Urasawa, O. Konno, A. Kagaya, R. Kato, T. Kamiyama, Y. Torizuka, T. Nanba, Y. Kondo, Y. Shibata, K. Ishi, T. Ohsaka, and M. Ikezawa, Phys. Rev. Lett. **63**, 1245 (1989).
[14]T. Nakazato, M. Oyamada, N. Niimura, S. Urasawa, R. Kato, Y. Shibata, K. Ishi, T. Ohsaka, T. Takahashi, H. Mishiro, M. Ikezawa, Y. Kondo, T. Nanba, and Y. Torizuka, Part. Accel. **33**, 141 (1990).
[15]Y. Shibata, K. Ishi, T. Ohsaka, H. Mishiro, T. Takahashi, M. Ikezawa, Y. Kondo, T. Nakazato, M. Oyamada, N. Niimura, S. Urasawa, R. Kato, and Y. Torizuka, Nucl. Instrum. Methods A **301**, 161 (1991).
[16]Y. Shibata, T. Takahashi, K. Ishi, F. Arai, H. Mishiro, T. Ohsaka, M. Ikezawa, Y. Kondo, T. Nakazato, S. Urasawa, R. Kato, S. Niwano, and M. Oyamada (unpublished).
[17]J. Schwinger, Phys. Rev. **75**, 1912 (1949).
[18]M. Sugawara, T. Ichinohe, S. Urasawa, M. Oyamada, T. Kubota, A. Kurihara, O. Konno, Y. Shibazaki, T. Terasawa, K. Nakahara, S. Nemoto, M. Muto, K. Shoda, and Y. Torizuka, Nucl. Instrum. Methods **153**, 343 (1978).
[19]For the beam dynamics in the injector, see R. H. Miller, in *The Stanford Two-Mile Accelerator,* edited by R. B. Neal (Benjamin, New York, 1968); R. H. Helm, R. Miller, P. Brunet, and X. Buffet, in *Linear Accelerators,* edited by P. M. Lapostolle and A. L. Septier (North-Holland, Amsterdam, 1970).
[20]S. Takeda, K. Tsumori, N. Kimura, T. Yamamoto, T. Hori, T. Sawai, J. Ohkuma, S. Takamuku, T. Okada, K. Hayashi, and M. Kawanishi, IEEE Trans. Nucl. Sci. **NS-32**, 3219 (1985).